Are the Ground States of the Later Actinocenes Multiconfigurational? All-Electron Spin−Orbit Coupled CASPT2 Calculations on An(η^8-C_8H_8)$_2$ (An = Th, U, Pu, Cm)

Andrew Kerridge and Nikolas Kaltsoyannis*

Department of Chemistry, University College London, 20 Gordon Street, London WC1H 0AJ, U.K.

Received: April 28, 2009; Revised Manuscript Received: June 15, 2009

Spin−orbit free and spin−orbit coupled CASPT2 wave functions and energies are presented for the ground and low-lying excited states of four actinide element sandwich molecules; thorocene ($ThCOT_2$), uranocene ($UCOT_2$), plutonocene ($PuCOT_2$), and curocene ($CmCOT_2$). Spin−orbit coupling is found to make little difference to the equilibrium geometry of uranocene and plutonocene but has a significant effect on the energy spectrum of all the systems considered here other than thorocene. In all cases, however, the spin−orbit free ground states make the dominant contribution to their spin−orbit coupled counterparts. Following work presented in *J. Phys. Chem. A* **2009**, *113*, 2896, the variation in the multiconfigurational character of the ground-state wave functions as the 5f series is crossed is quantified via the occupation of the a_u/b_{1u} (e_{2u}) metal-ring bonding and antibonding natural orbitals. The ground state of plutonocene is found to be nondegenerate with $|M_J| = 0$, in agreement with its temperature-independent paramagnetism.

1. Introduction

The lanthanocenes and actinocenes $MCOT_2$ (M = f element; COT = η^8-C_8H_8) are unique in organometallic chemistry in that only for these compounds is a structure of D_{8h} symmetry found, i.e., the metal center is sandwiched by planar and parallel carbocyclic rings in an eclipsed orientation. To date, Ce-,[1] Th-,[2] U-,[3] Np-,[4] and Pu-containing compounds[4] have been synthesized, along with $PaTMCOT_2$ (TMCOT = η^8-$C_8H_4(CH_3)_4$),[5] and data on their electronic, molecular, vibrational, and magnetic structure have been obtained.[1−14] Of these data, perhaps the most interesting are the magnetic properties of Ce- and $PuCOT_2$, both of which appear to display temperature-independent paramagnetism (TIP) at low temperatures.[12,14] In the former, the TIP has been considered in terms of a molecular Kondo-like effect.[15−17] Such an explanation requires an open-shell singlet electronic structure, leading to suggestions that the cerium ion may exist in a trivalent state, by contrast to its actinide analogue, thorium, which is clearly tetravalent in $ThCOT_2$. Although it is not universally accepted,[18] there is both experimental and theoretical evidence to support this view.[13,14,19−21] More specifically, previous computational studies from Dolg et al. concluded that the $^1A_{1g}$ ground-state wave function of cerocene is multiconfigurational, with a dominant (∼80%) ring $\pi^3f_\delta^1$ (Ce(III)) open-shell singlet configuration, and subsequent X-ray absorption spectroscopy experiments appear to support this trivalent picture.[13,14]

Very recently, we performed spin−orbit coupled complete active space self-consistent field calculations with dynamic correlation included via second order perturbation theory (hereby referred to as SOC-CASPT2) on $MCOT_2$ (M = Th, Pa, Ce),[22] and while our results for the actinide containing species were in excellent agreement with previous work, our data for cerocene were rather different from those of Dolg et al. We concluded that interpretations of the ground-state wave function in terms of the canonical CASSCF configurations is problematic, as the configurational admixture is not stable with respect to the computational methodology employed (specifically, the number of states included in the state averaging procedure). That said, we agreed with Dolg et al. that the cerocene ground state is multiconfigurational but preferred to use the occupation numbers of the natural orbitals as a quantitative measure of this effect. We found a total 4f density (n_f) of 0.90 ± 0.04, in excellent agreement with the experimentally determined value of 0.89 ± 0.03,[14] but this density is not due to the single occupation of a localized 4f orbital, as would be expected for a formally Ce(III) compound. Rather, it is due to significant partial occupation of orbitals exhibiting strong $\pi(e_{2u})/f_\delta$ covalency, and we suggested that the experimental conclusion of trivalent Ce is a function of the method measuring an effective, rather than a formal, oxidation state. We concluded that if we make the simple distinction that a genuinely Ce(III) compound would be expected to have a metal-localized f electron, while a Ce(IV) compound would not, then cerocene fits better into the latter category, notwithstanding its significant f density.

It is well-known that the chemistry of the later actinides is rather different from that of the early members of the series, with the variable valence of the latter being replaced by a dominant lanthanide-like trivalent oxidation state.[23] Dolg and Fulde[24] have previously suggested that the electronic structures of the actinocenes should therefore change from single-configurational An(IV) behavior, as exemplified by thorocene ($ThCOT_2$), to become more cerocene-like as the middle of the series is approached. In the present contribution, we extend our earlier work to three more actinocenes, uranocence ($UCOT_2$), plutonocene ($PuCOT_2$), and curocene ($CmCOT_2$), to probe this suggestion, particularly in the light of our recent conclusions concerning cerocene. For completeness, we also present a summary of our results for $ThCOT_2$ from reference 22.

2. Computational Details

All calculations were performed using the MOLCAS 6.4 code.[25] Spin−orbit free (SOF-) and spin−orbit coupled (SOC-)-CASPT2 calculations were performed using all-electron ANO

* To whom correspondence should be addressed. E-mail: n.kaltsoyannis@ucl.ac.uk.

10.1021/jp903912q CCC: $40.75
Published on Web 07/02/2009

basis sets for all atoms and incorporating scalar relativistic effects via the second-order Douglas−Kroll Hamiltonian.[26] The basis sets used were as follows. For the metal atoms, correlation-consistent basis sets, constructed by Roos,[27] were employed, contracted as (27s24p18d14f)/[10s9p7d5f]. These bases are of approximate VQZ quality. For C and H, ANO basis sets of DZP quality were used. We have previously shown[22] that the exclusion of polarizing g functions in our metal basis and/or improvements in the ligand basis do not significantly alter the multiconfigurational character of the cerocene, thorocene, or protactinocene ground states nor the relative energies of the ground and low-lying excited states.

Reference orbitals for the CASSCF calculations were generated from restricted Hartree−Fock (RHF) calculations using the basis sets described above. The improved virtual orbital (IVO) method[28] was used to generate more compact virtual orbitals than would be obtained from RHF calculations.

In all calculations, the COT rings were assumed to be planar and of D_{8h} symmetry, with $r_{CC} = 1.404$ Å and $r_{CH} = 1.087$ Å, as used in previous work.[19,22,29] This ring structure was held fixed during numerical optimisation of the metal−COT ring centroid distance at the CASPT2 level. We have previously performed a full geometry optimization of the ground state of $ThCOT_2$ in Gaussian 03[30] using density functional theory with the B3LYP exchange correlation functional (see reference 22 for details) giving $r_{CC} = 1.416$ Å and $r_{CH} = 1.093$ Å. Such minor deviations from our assumed ring structure will have only minimal effects on electronic properties.

Restrictions of MOLCAS 6.4 require the calculations to be performed under D_{2h} symmetry. Bearing this in mind, we use the irreducible representations (irreps) of this point group in our discussions. This is necessary since, in the subduction from D_{8h} to D_{2h} symmetry, certain formally orthogonal orbitals are allowed to mix. In terms of metal d and f levels, mixing of d_σ ($m_l = 0$) and d_δ ($m_l = \pm 2$), f_σ ($m_l = 0$) and f_δ ($m_l = \pm 2$), and f_π ($m_l = \pm 1$) and f_ϕ ($m_l = \pm 3$) can (in principle, at least) occur. Where relevant, we also use the irreps of D_{8h} to aid comparison with previous work. When this is the case, the representation in D_{8h} follows that in D_{2h} and is enclosed in parentheses.

All data presented in section 3 were obtained from state-averaged CASSCF calculations, where the state average is taken over the ground and first excited states of a given spatial and spin symmetry for thorocene and uranocene and over the ground and first two excited states for plutonocene and curocene. The inclusion of the higher excited states in calculations of the latter systems reflects the increased density of states associated with higher f orbital occupation. As well as reducing the likelihood that the states obtained are local, rather than global, minima, averaged states lead to more reliable spin−orbit coupling results. Such results are known to be highly sensitive to state overlap,[31] which can be non-negligible in the absence of state averaging. It should be stressed, however, that all discussion and analysis of natural orbitals and their occupations[32] uses the true natural orbitals for the state under consideration as opposed the pseudonatural orbitals derived from the state-averaged electron density (as are generated by default in MOLCAS).

The SOF-CASSCF calculated states were used as a basis for SOC calculations. These calculations were performed using the restricted active space state interaction (RASSI) formalism.[33] State energies were adapted according to the SOF-CASPT2 results. In the double point group D_{2h}^*, the direct product $\Gamma_{g,u} \times E_{1/2g} = E_{1/2g,u}$ for any irrep Γ of D_{2h}, and so for clarity we list the D_{2h} SOF states of which the SOC states are composed in our discussions. Where possible, we infer symmetry labels for spin−orbit coupled states from previous work.

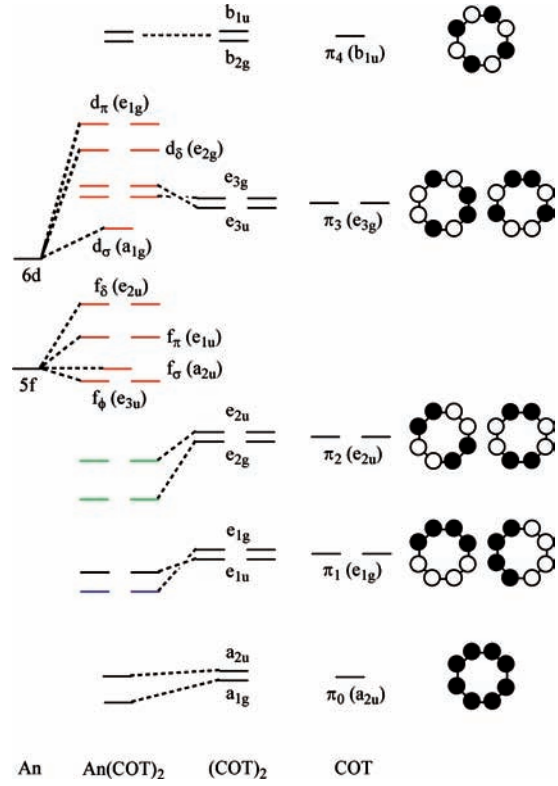

Figure 1. Qualitative molecular orbital energy level diagram for an early actinocene. Green levels are occupied ligand levels included in all active spaces used in this study. Blue levels are occupied ligand levels included only in the 16 orbital active spaces. Red levels are metal and unoccupied ligand levels that can be partially occupied in the active spaces.

2.1. Active Spaces. In moving from thorocene to curocene, different computational demands presented themselves, and so we chose different active spaces to reflect this. For thorocene and uranocene, the ring centroid-metal separations have been experimentally determined, and so for these molecules we used the largest computationally tractable active space we could for the optimization of this distance. For thorocene, this active space explicitly correlates 12 electrons in 16 orbitals, for which we adopt the notation CASSCF(12,16) (or CASPT2(12,16)). The nature of this active space can be best understood with reference to Figure 1, a qualitative molecular orbital energy level diagram for an early actinocene. Of the 16 orbitals, 6 were doubly occupied in the RHF-IVO reference calculation. This active space was used to ensure that the role of valence d levels in bonding was properly accounted for; in addition to the highest-lying a_g and b_{1g} (e_{2g}), and a_u and b_{1u} (e_{2u}) ring-based occupied levels (shown in green in Figure 1), whose inclusion in the active space is standard in previous work,[19,29,34−36] the lower-lying b_{2g} and b_{3g} (e_{1g}) levels (shown in blue in Figure 1) were included, ensuring that d_σ, d_δ, and f_δ electrons, which span these irreps, were all well correlated. Although this active space allows for occupation of any f orbital, it does not allow occupation of both the f_σ and one of the f_δ orbitals, since in D_{2h} these orbitals span the same irrep, b_{1u}. A (12,17) active space would be sufficient to allow this particular occupation but proved to be computationally intractable. There are two situations in which this lack of flexibility in the active space could be problematic. The first corresponds to a state in which both the b_{1u} f_σ and f_δ orbitals were occupied. The second would arise

only in a state-averaged calculation in which one state involved the occupation of the f_σ orbital and another involved the occupation of the f_δ. Neither of these situations is of concern in our thorocene calculations; the f^2 configuration would correspond to a highly excited divalent state, of no interest here, and the f_δ level lies significantly higher in energy than any other f level (on account of the principal metal-ring interaction being via the e_{2u} ring π and f_δ levels) and so would never be occupied in small state-averaged calculations as have been performed here.

While this large active space was used for the numerical metal-ring centroid optimisation, we reduced its size for our studies of the thorocene ground and low-lying excited states for computational efficiency. This reduction was straightforward and involved the removal of the occupied b_{2g} and b_{3g} (e_{1g}) ligand levels. This (8,14) active space reduced the cost of calculations significantly, while excluding from the configuration space only configurations corresponding to excitations from deep-lying ligand levels. This reduction was therefore expected to have minimal impact on our results and would in any case be partially corrected by the perturbational treatment of the dynamic correlation.

The active spaces used in the uranocene calculations are essentially the same as those of thorocene, the difference being the inclusion of two additional electrons such that the partial optimizations were performed at the CASPT2(14,16) level, with subsequent calculations at the CASPT2(10,14) level. Again, neither of the two potential problems with the active spaces discussed above is of concern here; although an f^2 configuration corresponds to tetravalent uranium, the relatively high energy of the f_δ level means that states involving its occupation would lie high in energy, and so would not appear in our calculations.

The situation is somewhat different for plutonocene. Another two electrons must be added to the active space, and CASPT2(16,16) calculations (as would be required for the partial geometry optimization, by extension of the larger $ThCOT_2$ and $UCOT_2$ active spaces) are currently beyond our capabilities. On the other hand, we were concerned that a 14 orbital active space, as employed in the smaller $ThCOT_2$ and $UCOT_2$ calculations, would not be large enough on the grounds that the more contracted 5f orbitals of plutonium would be perturbed less by the COT_2 ligand field than in $ThCOT_2$ and $UCOT_2$, such that we should allow for simultaneous f_σ/f_δ occupation. We therefore added another b_{1u} orbital to the 14 orbital active space and performed partial optimizations and subsequent ground- and excited-state calculations at the CASPT2(12,15) level. The situation was expected to be similar (if not more pronounced) for curocene, and so in this case both optimisations and ground-state calculations were performed at the CASPT2(14,15) level.

3. Results

3.1. Thorocene. ***3.1.a. SOF Calculations.*** We have reported fully our results on thorocene in a previous study[22] and so will only briefly summarize them here. A total of 32 states were calculated at the SOF-CASPT2 level, these being the two lowest energy states of each of the eight irreps of the D_{2h} point group for both the singlet and triplet spin multiplicities. The SOF ground state was found to be of ^1A_g ($^1A_{1g}$) symmetry, and the SOF-CASPT2(12,16) calculated equilibrium ring-metal separation was found to be 2.015 ± 0.001 Å, in excellent agreement with the experimentally observed value of 2.004 Å[2]. (The error of ± 0.001 Å in the calculated ring-metal separation arises as the numerical optimization was performed using a set of points separated by this distance. This is also the case for all other systems considered in this study). All SOF-CASPT2(8,14) calculations were performed at this equilibrium geometry. At the SOF-CASPT2(8,14) level, the ^1A_g ($^1A_{1g}$) remained the ground state, corresponding to a d^0f^0 Th(IV) configuration and lying 2.47 eV below the next-lowest-lying level, a doubly degenerate level of $^1A_u/^1B_{1u}$ ($^1E_{2u}$) symmetry, corresponding to a d_σ^1 Th(III) configuration. As we have previously noted, the energetically preferential occupation of $6d_\sigma$ level over any f orbital is chemically reasonable; while trivalent thorium compounds are rare, $ThCp_3$" (Cp" = $C_5H_3(SiMe_3)_2$), has been shown both experimentally[37] and theoretically[38] to have a d_σ^1 ground configuration.

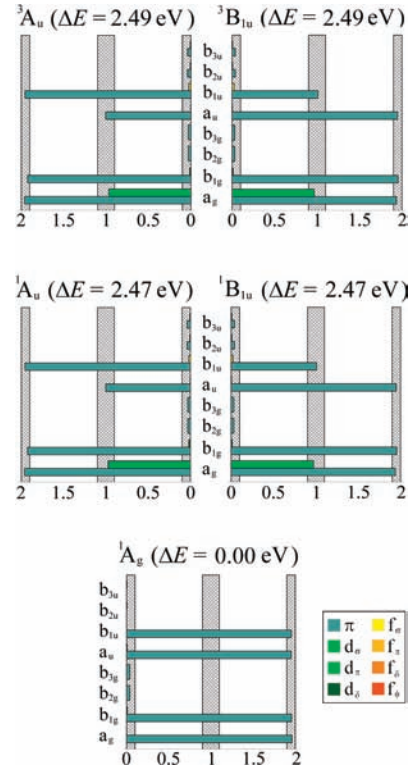

Figure 2. Active space natural orbital occupations for the lowest-lying SOF-CASPT2(8,14) calculated states of $ThCOT_2$. Bars terminating outside of the crosshatched areas indicate strong multiconfigurational character.

The natural orbital occupations (NOOs) of the lowest-lying SOF states of thorocene are shown in Figure 2. NOOs can be taken as an indicator of multiconfigurational character; integer (or zero) occupation of all orbitals corresponds to a single configuration wave function, whereas occupations deviating by greater than 0.1 from integer values are an indicator of strong multiconfigurational character.[39] Figure 2 shows that the ground and low-lying excited states are all well described by a single configuration wave function, and also clarifies the nature of the difference between the ground and low-lying excited states, namely, the deoccupation of a ligand a_u/b_{1u} (e_{2u}) level. Singlet and triplet excited states have near identical NOOs, unsurprising given that the triplet states lie at 2.49 eV above the ground state, just 0.02 eV higher than the singlets.

3.1.b. SOC Calculations. The 32 SOF-CASPT2 states were used as a basis for spin−orbit coupled calculations, performed using the RASSI state interaction method, and Figure 3 shows the energies of the lowest-lying SOF and SOC states (and also displays the compositions of the latter in terms of the SOF states). The effect of spin−orbit coupling on the state energies is clearly small, e.g., the ground state is stabilized by 0.02 eV

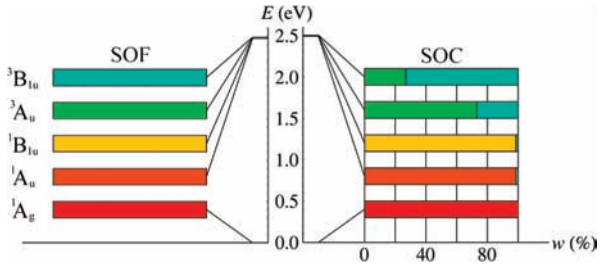

Figure 3. Ground and low-lying excited states of $ThCOT_2$ calculated at the CASPT2(8,14) level both spin−orbit free (left-hand side) and with the inclusion of spin−orbit coupling (right-hand side). The color coding shows the compositional weight (w) of the spin−orbit coupled states in terms of the principal spin−orbit free states.

relative to the first excited state (2.49 vs 2.47 eV at the SOF-CASPT2 level).

Experimentally, "a broadband of low intensity...centered at 450 nm (2.76 eV) with a shoulder at shorter wavelength" is observed in the UV−visible spectrum of $ThCOT_2$.[40] In our SOF-CASPT2 calculations, we find the lowest energy ungerade states, $^1A_u/^1B_{1u}$ ($^1E_{2u}$), to lie 2.47 eV above the ground state (rising to 2.49 eV at the SOC level), with the corresponding triplet states lying ~0.02 eV above this. Although transition to this state is formally dipole-forbidden in D_{8h} symmetry, it seems highly likely that the experimentally observed band is indeed due to transitions to the ungerade states located at ~2.5 eV; the next ungerade states in our calculations lie some 2 eV higher in energy. We therefore suggest that the purely electronic ring $\pi(e_{2u}) \rightarrow d_\sigma$ transitions become weakly allowed through coupling to vibrational modes which lower the point group of the system to D_{2h} (such couplings will also account for the broadness of the experimental peak). In our previous study, we presented possible vibrational modes which could effect this non-zero intensity.[22]

3.2. Uranocene. ***3.2.a. SOF Calculations.*** 32 states were calculated at the SOF-CASPT2 level, these being the two lowest energy states of each of the eight irreps of the D_{2h} point group, for both the singlet and triplet spin multiplicities. The SOF ground state was found to be doubly degenerate, of $^3A_g/^3B_{1g}$ ($^3E_{2g}$) symmetry. The SOF-CASPT2(14,16) equilibrium ring-metal separation was found to be 1.944 ± 0.001 Å, in good agreement with the experimentally observed value of 1.924 Å.[2] (Note that in our previous publication we erroneously stated that we had calculated the U-COT centroid separation to be 1.926 Å.[22]) All subsequent SOF-CASPT2(10,14) calculations were performed at this equilibrium geometry, and at this level, the $^3A_g/^3B_{1g}$ ($^3E_{2g}$) state, corresponding to a $f_\pi^1 f_\phi^1$ U(IV) dominant configuration, remained lowest in energy.

Figure 4 shows the NOOs for the ground and lowest-lying excited states, from which it can be seen that there is a marked difference between the uranocene SOF ground state and that of thorocene, the former appearing to have strong multiconfigurational character. However, this is a consequence of the symmetry of the ground state. Both the f_π and f_ϕ levels are doubly degenerate in both D_{2h} and D_{8h} symmetry, and consequently there are two $f_\pi^1 f_\phi^1$ uranium configurations that can contribute to a state of ^3A_g symmetry (and similarly for $^3B_{1g}$). The most general multiconfigurational wave function of this symmetry then takes the form of a linear combination of these configurations, from which the NOOs in Figure 4 follow. We therefore conclude that although the SOF-CASPT2 calculated uranocene ground state appears to be strongly multiconfigurational, it is very different from the genuinely multiconfigurational state we find in our cerocene calculations.[22]

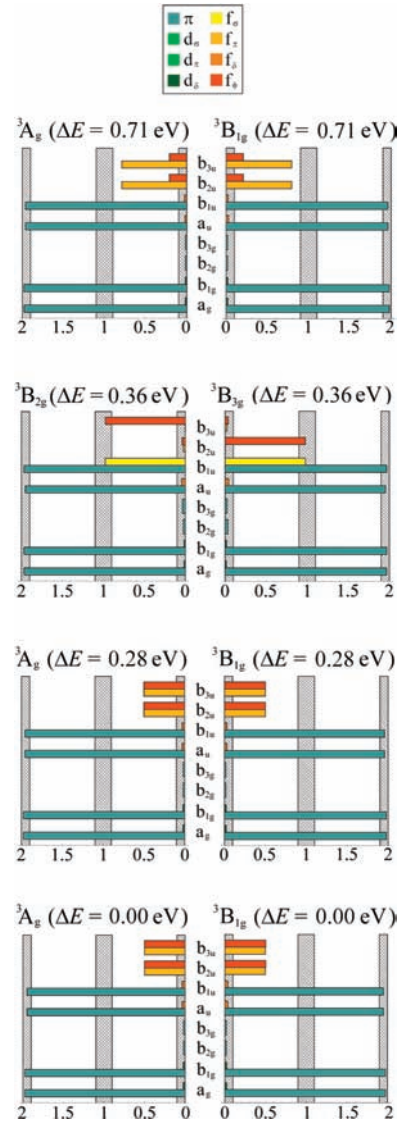

Figure 4. Active space natural orbital occupations for the lowest-lying SOF-CASPT2(10,14) calculated states of uranocene. Bars terminating outside of the crosshatched areas indicate strong multiconfigurational character.

An interesting feature of the SOF ground state is the weak occupation of the a_u/b_{1u} (e_{2u}) f_δ natural orbitals. In cerocene, the significant occupation (0.216) of each of these orbitals in the ground state is a manifestation of a strongly multiconfigurational wave function and leads to the large f density for what we characterize to be a formally tetravalent system.[22] In uranocene this occupation is much weaker (0.036) but is significantly larger than in thorocene, where the occupation is negligible (0.006). We identify this occupation with the onset of the multiconfigurational character that we are looking for in the later actinocenes.

We now consider the other SOF states presented in Figure 4. The first excited state, lying 0.282 eV above the ground state, is again doubly degenerate and of $^3A_g/^3B_{1g}$ ($^3E_{2g}$) symmetry and also corresponds to linear combinations of uranium $f_\pi^1 f_\phi^1$ configurations. In this case the states are antisymmetric combinations of these configurations, as opposed to the symmetric combinations comprising the ground state. At higher energy (ΔE = 0.359 eV) is another doubly degenerate state which is clearly single configurational and corresponds to a $f_\sigma^1 f_\phi^1$ uranium configuration. Finally, at an energy 0.708 eV above the ground

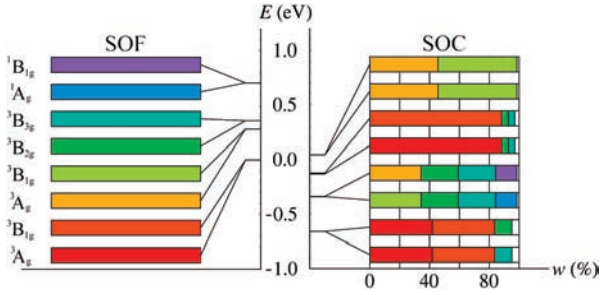

Figure 5. Ground and low-lying excited states of $UCOT_2$ calculated at the CASPT2(10,14) level both spin−orbit free (left-hand side) and with the inclusion of spin−orbit coupling (right-hand side). The color coding shows the compositional weight (w) of the spin−orbit coupled states in terms of the principal spin−orbit free states.

TABLE 1: Comparison of the Composition (in Terms of the Weight of the Spin−Orbit Free State Admixture) of the Uranocene Spin−Orbit Coupled Ground State Calculated Here (at Both the CASSCF and CASPT2 Levels) with That Obtained at the SOCI Level in Ref 35

			weight (%)		
state	dominant configuration	spin	SOCI	SOC-CASSCF	SOC-CASPT2
$^3A_g/^3B_{1g}$	$f_\pi^1 f_\phi^1$	1	68.0	70.7	83.7
$^3B_{2g}/^3B_{3g}$	$f_\sigma^1 f_\phi^1$	1	22.7	22.1	11.4
$^1B_{2g}/^1B_{3g}$	$f_\sigma^1 f_\phi^1$	0	5.3	7.0	4.6
	$f_\pi^1 f_\delta^1$	1	2.3	not included	not included
	$f_\sigma^1 f_\delta^1$	1	1.1	not included	not included
	$f_\pi^1 f_\delta^1$	0	0.6	not included	not included

state is a doubly degenerate singlet state of $^1A_g/^1B_{1g}$ ($^1E_{2g}$) symmetry, which can be considered to be the singlet equivalent of the SOF ground state. However, the multiplicity of this state allows configurations incorporating double occupation of f levels, and the significant difference in the NOOs of this state in comparison with the ground state is due to a configuration involving double occupation of the f_π level.

3.2.b. SOC Calculations. The 32 SOF states were used as a basis for SOC-CASPT2 calculations. By contrast to thorocene, the effects of spin−orbit coupling in uranocene are considerable. Figure 5 presents the relative energies of low-lying SOF and SOC states and also depicts the composition of the SOC states in terms of the SOF basis. The higher density of states for this and latter systems means that our calculated SOC states may have components from higher-lying SOF states, which we have indicated as uncolored contributions to the SOC states. The SOC ground state is stabilized by 0.663 eV relative to its SOF counterpart, although the increase in ground-state stabilization relative to the first excited is more modest, 0.321 eV at the SOC-CASPT2 level compared with 0.282 eV at the SOF-CASPT2 level. The SOC ground state is a strong admixture of low-lying SOF states, and Table 1 contains a comparison of our results with those of Chang and Pitzer,[35] performed at the spin−orbit coupled configuration interaction (SOCI) level of theory. To aid comparison with these latter data, we include our results obtained using both the SOF-CASSCF and SOF-CASPT2 energies as input for the spin−orbit coupling calculation. The SOC-CASSCF results would be expected to be in better agreement with the SOCI results, since both methods neglect dynamic correlation, and this is indeed the case. While our 32-state basis does not include every state found in the E_{3g} $|M_J| = 4$ SOCI ground state, it does include the three major contributions, and the agreement between the SOCI and SO-CASSCF results is very good, especially when taking into account the different geometries used in the two calculations; reference 35 uses the experimentally determined ring-metal separation. We therefore infer an E_{3g} ground state with $|M_J| = 4$. When the effects of dynamical correlation are taken into account, the contribution of the dominant SOF state to the SOC ground state is increased, mainly at the expense of the secondary SOF state.

Experimentally reported peaks in the UV/vis spectrum of uranocene occur at 1.880, 1.934, and 2.018 eV.[8] It is also known[6] that the second is xy polarized and the third z polarized. At the SOC-CASPT2 level we calculate an optically allowed z-polarized transition at 1.79 eV with oscillator strength $f = 0.0027$ and an allowed xy polarized transition at 1.65 eV with oscillator strength $f = 0.0018$. Both of these transitions principally involve an $f_\pi \rightarrow d_\sigma$ transition. All other calculated excited states have oscillator strengths at least an order of magnitude smaller. The disagreement with experiment is 0.2−0.3 eV, a similar level of accuracy to that found in our previous study.[22]

3.3. Plutonocene. ***3.3.a. SOF Calculations.*** We have calculated 48 plutonocene states at the SOF-CASPT2 level, these being the three lowest energy states of each of the eight irreps of the D_{2h} point group, for both the triplet and quintet spin multiplicities. The number of states of each symmetry and multiplicity was increased from two to three to reflect the higher density of states involving f level occupation in this system. As discussed in section 2.1, and in light of the weak occupation of the a_u/b_{1u} (e_{2u}) metal-based levels in uranocene, a single active space was employed for both partial geometry optimizations and subsequent state-averaged calculations. In comparison with the 14 orbital active space employed for the bulk of the $ThCOT_2$ and $UCOT_2$ calculations, a virtual orbital of b_{1u} symmetry was added. The SOF-CASPT2(12,15) ground state was found to be nondegenerate, and of ^5A_g ($^5A_{1g}$) symmetry. The energy of this state was minimized at a ring-metal separation of 1.898 ± 0.001 Å, and this geometry was used for all subsequent calculations. Detailed structural information for this compound is not available, but an approximate ring metal separation can be deduced by scaling the values known experimentally for thorocene and uranocene by the ratios of the ionic radii of Th^{4+} and U^{4+} to Pu^{4+}.[41] This procedure yields a value of 1.83 Å when using the Th^{4+}/Pu^{4+} ratio and 1.86 Å when using the U^{4+}/Pu^{4+} ratio. These approximate values compare reasonably well with our calculated value and suggest a continuation of the trend of a small overestimation of ring-metal separations at the SOF-CASPT2 level.

Figure 6 shows the NOOs of the ground and low-lying excited SOF-CASPT2 plutonocene states. The ^5A_g ($^5A_{1g}$) ground state has near integer occupancy of four f levels, corresponding to an $f_\pi^2 f_\phi^2$ plutonium configuration, but also has significant (0.183) occupation of the a_u/b_{1u} (e_{2u}) f_δ levels, largely due to partial deoccupation (to 1.849) of the corresponding $\pi(e_{2u})$ levels. This occupation, some five times larger than that found in uranocene, bears a striking resemblance to that of cerocene, where the equivalent occupation is 0.216 (and 1.751 for the corresponding π levels). We therefore conclude that, at the SOF level at least, the electronic structure of the plutonocene ground state can be characterized in the same way as that of cerocene, as suggested by Dolg and Fulde,[24] and from the multiconfigurational point of view the metal-dominated a_u/b_{1u} (e_{2u}) $5f_\delta$ levels are acting as correlating orbitals to the ring based $\pi(e_{2u})$ levels.

The SOF plutonocene ground state lies 0.182 eV below the doubly degenerate $^5B_{2g}/^5B_{3g}$ first excited state. This state is strongly multiconfigurational, but can be to some extent characterized in terms of an $f_\pi \rightarrow f_\sigma$ transition, and so would appear to be dominated by an $f_\sigma^1 f_\pi^1 f_\phi^2$ plutonium configuration.

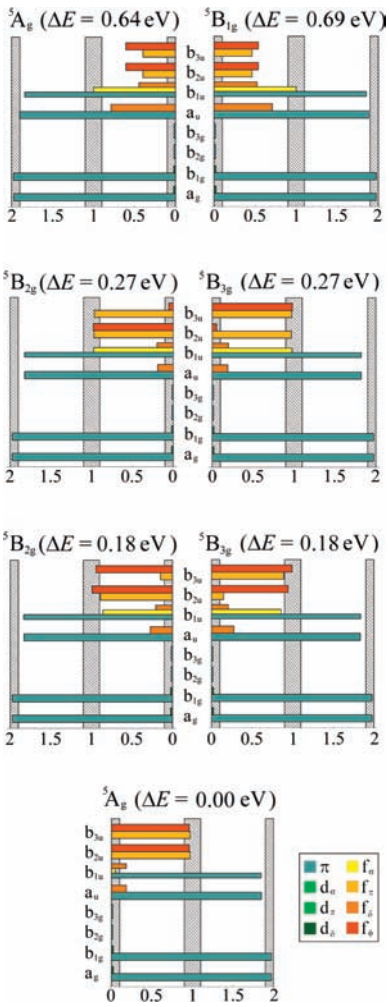

Figure 6. Active space natural orbital occupations for the lowest-lying SOF-CASPT2(12,15) calculated states of plutonocene. Bars terminating outside of the crosshatched areas indicate strong multiconfigurational character.

The next lowest-lying state (ΔE = 0.266 eV) is again doubly degenerate and of $^5B_{2g}/^5B_{3g}$ symmetry, but here the multiconfigurational character is less strongly pronounced, notwithstanding the still significant a_u/b_{1u} (e_{2u}) f_δ occupation, and so this state can be characterized by a dominant $f_\sigma^1 f_\pi^2 f_\phi^1$ plutonium configuration. The final state depicted in Figure 6 is the strongly multiconfigurational and formally doubly degenerate $^5A_g/^5B_{1g}$ ($^5E_{2g}$) state, lying 0.663 eV above the ground state. Unfortunately, due to the type of state averaging that we can perform using MOLCAS, the two components of this state are not degenerate in our calculations, differing in energy by 0.056 eV at the SOF-CASPT2 level. A corresponding difference in NOOs can be observed in Figure 6, but the broad similarity of the states allows us to deduce their degeneracy. The source of this error in our calculations comes from the restrictions of working in D_{2h} symmetry; the state average yielding the ^5A_g component of this (D_{8h}) $^5E_{2g}$ state also contains a state of (D_{8h}) $^5A_{1g}$ symmetry, which the $^5B_{1g}$ component cannot. While this discrepancy could be avoided by performing a smaller state average on the ^5A_g component, the orthogonality of this component to the ground state would then be lost. In any event, this symmetry breaking appears to have a negligible effect on the calculated SOC spectrum.

3.3.b. SOC Calculations. The 48 SOF states were used as a basis for the SOC-CASPT2 calculation, and the results are presented in Figure 7. As with uranocene, the effects of spin−orbit coupling are large; the SOC ground state lies 0.76 eV below its SOF counterpart, although it is destabilized with respect to the first excited state. At the SOF-CASPT2 level the ground state is stable by 0.18 eV, reducing to 0.09 eV with the inclusion of spin−orbit coupling.

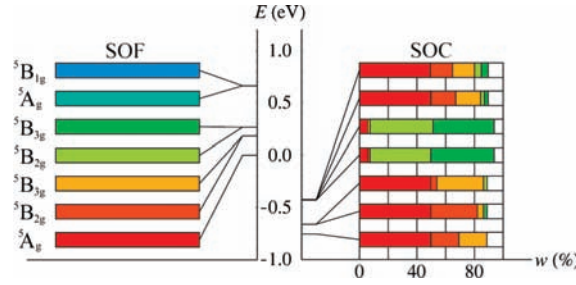

Figure 7. Ground and low-lying excited states of $PuCOT_2$, calculated at the CASPT2(12,15) level both spin−orbit free (left-hand side) and with the inclusion of spin−orbit coupling (right-hand side). The color coding shows the compositional weight (w) of the spin−orbit coupled states in terms of the principal spin−orbit free states.

Figure 7 shows that the SOC-CASPT2 ground state is nondegenerate, defining it as an A_{1g} state with $|M_J| = 0$ in D_{8h}* symmetry, in agreement both with previous SOCI calculations[36] and analysis based on crystal field theory.[4,42,43] The identification of this $|M_J| = 0$ ground state is consistent with the TIP reported in ref 12.

Experimentally observed UV/vis absorption peaks occur for plutonocene at 2.768, 2.995, and 3.069 eV.[9] Our SOC-CASPT2 calculations give a large number of excited states with non-negligible oscillator strengths; the most strongly allowed of the low-lying states are found at 3.328 (f = 0.034), 3.556 (f = 0.0017), and 3.705 eV (f = 0.0017). While the energetic separation of these states is in general agreement with those observed experimentally, the overall inaccuracy in the excitation energies of c. 0.5 eV, combined with the large number of less strongly allowed transitions, leave us reluctant to attempt an assignment of the experimentally observed transitions.

3.4. Curocene. ***3.4.a. SOF Calculations.*** The final system considered in this study is curocene, $CmCOT_2$. Since this compound has not been synthesized and our main goal in this study is to understand the ground-state electronic structures of the actinocenes, we restricted our calculations for this system to states of gerade parity. (The large energy separation between states of gerade and ungerade parity found for all other systems in this study justifies this approach. Furthermore, the difficulties associated with the assignment of the experimentally determined absorption peaks in plutonocene suggest that any attempt to predict accurate excitation energies for curocene would be unrewarding.) We calculated 24 states at the SOF-CASPT2(14,15) level, these being the three lowest energy states of each even parity irrep of D_{2h} for both the quintet and septet multiplicities. We found a doubly degenerate ground state of $^7A_g/^7B_{1g}$ ($^7E_{2g}$) symmetry at an equilibrium ring-metal separation of 1.922 ± 0.001 Å, a slight increase over that found in plutonocene. While this increase is arguably rather surprising, there is both experimental[44−46] and theoretical[47] evidence for an unusually large lattice constant in bulk CmO_2, for which the formal oxidation state of Cm is IV. Although the experimentally determined CmO_2 lattice constant is shorter than that of PuO_2, it is not as short as might be expected on extrapolation of the values of the early actinides, and DFT calculations give a marginally larger value for CmO_2 than PuO_2. This is attributed to an (albeit overemphasized) increase in spin-density on the Cm(IV) ion in order to approach the stability of the half-filled

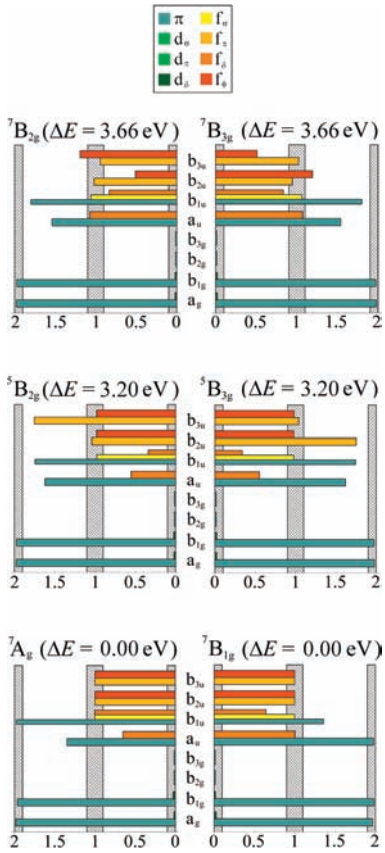

Figure 8. Active space natural orbital occupations for the low-lying SOF-CASPT2(14,15) calculated states of curocene. Shown here are the ground and first excited states, along with the next lowest-lying septet state. Bars terminating outside of the crosshatched areas indicate strong multiconfigurational character.

f^7 subshell.[47] As will be discussed later in this section, we find a similar increase in f density for $CmCOT_2$ over $PuCOT_2$, and so our results seem to corroborate this conclusion.

The identification of a $^7A_g/^7B_{1g}$ ($^7E_{2g}$) SOF ground state in this system is unsurprising. If we consider a simple single-configurational picture and assume curocene to contain a formal Cm(IV) high-spin f^6 center along with doubly occupied ligand levels, then the overall symmetry of the system is dictated by the hole in the half-filled Cm 5f shell. As indicated in Figure 1, we consider the 5f orbitals in the actinocenes to form a set of five lower-lying levels (f_σ, f_π and f_ϕ), with the remaining doubly degenerate f_δ pair, of a_u/b_{1u} (e_{2u}) symmetry, lying significantly higher in energy. This picture clearly suggests that the energetically most favorable f^6 state involves an unoccupied f_δ level. If this unoccupied level is of a_u symmetry in D_{2h}, the overall state will be A_g. Likewise, if it is of b_{1u} symmetry, the overall state will be B_{1g}. From this it follows that we should expect the $^7A_g/^7B_{1g}$ ($^7E_{2g}$) state to be very stable with respect to the first excited state, since any single-configurational state of any other symmetry will involve the occupation of both of the energetically unfavorable f_δ levels.

Figure 8 shows the NOOs of the SOF ground state and the lowest state of quintet and septet multiplicities and indicates that although the simple picture developed above is complicated by the multiconfigurational character of the actual ground-state wave function, it is broadly supported by our calculations. The SOF ground state displays near integer occupation of six f levels but also indicates extremely strong multiconfigurational character among the a_u/b_{1u} (e_{2u}) orbitals. The occupation of the seventh f level is 0.646. This is at first sight much higher than we have found for either cerocene or plutonocene but should be tempered by the fact that for each component of the doubly degenerate ground state, only one f_δ level is available for partial occupation, by contrast to the two available in the cerium and uranium systems. It is therefore more sensible to consider a value of 0.646/2 = 0.323 to compare with the a_u/b_{1u} (e_{2u}) occupations in the other actinocenes (see Table 2). Thus curocene is seen to continue the trend of increasing multiconfigurational character to the ground state as the 5f series is crossed, and indeed to exceed that of cerocene.

TABLE 2: Natural Occupations of the a_u/b_{1u} (e_{2u}) f_δ Orbitals in the Ground States of the Four Actinide-Containing Systems Considered in This Study, along with Those Found Previously for $PaCOT_2$ and $CeCOT_2$[22]

System	*n*
$ThCOT_2$	0.006
$PaCOT_2$	0.014
$UCOT_2$	0.036
$PuCOT_2$	0.183
$CmCOT_2$	0.323[a]
$CeCOT_2$	0.216

[a] The value quoted for $CmCOT_2$ is obtained by dividing a single orbital occupation by two for the purposes of comparison. See main text for details.

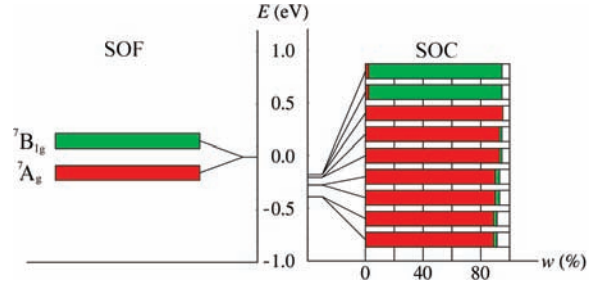

Figure 9. Ground and low-lying excited states of $CmCOT_2$, calculated at the CASPT2(14,15) level both spin−orbit free (left-hand side) and with the inclusion of spin−orbit coupling (right-hand side). The color coding shows the compositional weight (*w*) of the spin−orbit coupled states in terms of the principal spin−orbit free states.

The first excited SOF state of curocene lies 3.20 eV above the ground state and is of $^5B_{2g}/^5B_{3g}$ symmetry. The quintet multiplicity allows for the double occupation of f levels, and the main difference between this excited state and the ground state is a significant reduction in f_δ occupation, along with a corresponding increase in f_π occupation from 1.00 to 1.75. Figure 8 also shows the NOOs of the lowest energy excited septet state ($^7B_{2g}/^7B_{3g}$), lying 3.66 eV above the ground state. In a single-configurational picture, this state would correspond to an occupation of both f_δ levels, with the deoccupation of either an f_π or f_ϕ level. In the multiconfigurational wave function calculated here, this restriction is somewhat relaxed. The NOOs can have occupations greater than 1, and so, while an overall increase in the f_δ occupations is found, the energetically unfavorable full occupation of both levels is reduced by an increased fractional occupation of other f levels, along with the significant deoccupation of the f_ϕ level, resulting in a strongly multiconfigurational state.

3.4.b. SOC Calculations. The large relative stability of the curocene SOF ground state suggests that the excited states will play only minor roles in the low-lying SOC states. As can be seen in Figure 9 this is indeed the case. The density of states around the SOC ground state is much higher than in the SOF system, with the first 14 states being separated by just 0.31 eV.

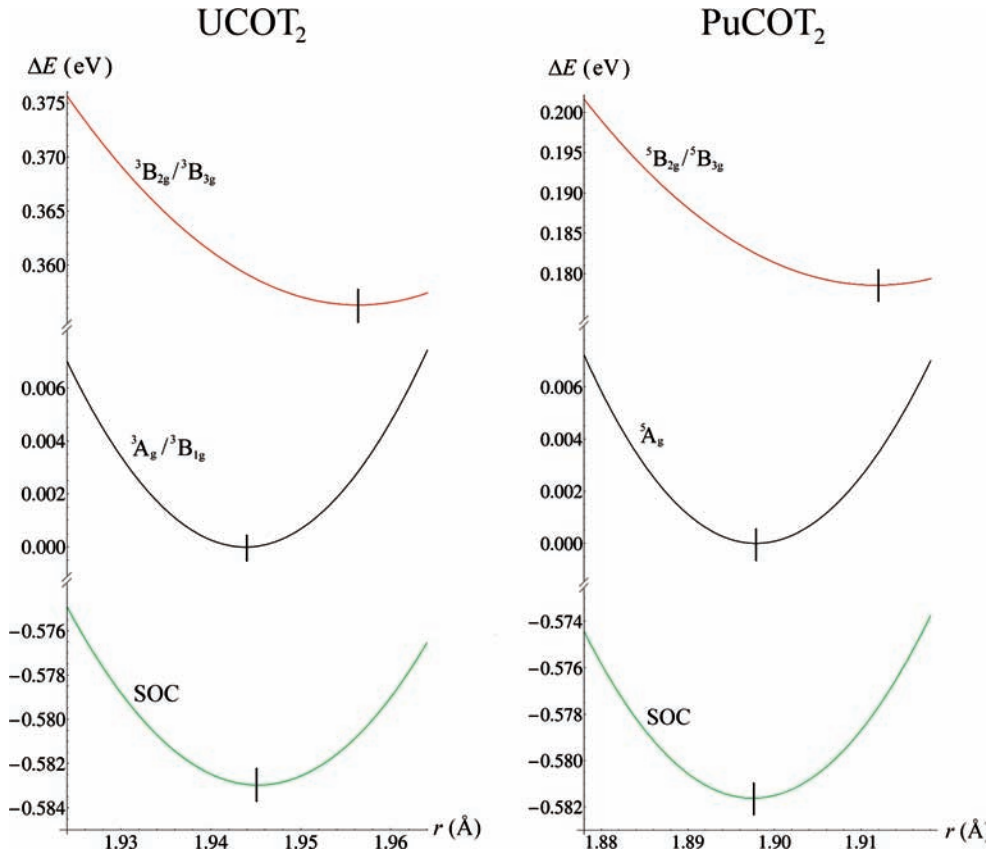

Figure 10. Potential energy curves for the metal-ring centroid distance in the $UCOT_2$ and $PuCOT_2$ SOC ground states and contributing SOF states. Vertical black bars indicate minima. All energies are relative to the equilibrium SOF ground-state energy.

The SOC ground state is 0.39 eV lower in energy than its SOF counterpart and is stable by 0.11 eV relative to the first excited state.

3.5. Spin−Orbit Coupled Optimisation of the Metal-Ring Centroid Distance in Uranocene and Plutonocene. There is evidence to suggest that the incorporation of spin−orbit coupling into geometry optimizations of closed shell heavy element complexes has little effect,[48] but it might be expected that spin−orbit coupling would be more significant for open-shell systems: the inclusion of spin−orbit coupling results in an increase of 0.002 Å in the calculated Pu−O bond length of PuO_2^{2+} and an increase of 0.001 Å in the Pu−N bond length of PuN_2 at the CASPT2 level of theory,[49] while a study of PuO and PuO_2 in a variety of charge states[50] finds that bond length variations of the order of 0.001 Å are typical at the SOC-CASPT2 level. Similar effects were found in a SOC-CASPT2 study of $DyBr_3$.[51] As an example of the effect as calculated using density functional theory, the U−C bond length in I_3U−CO is increased by 0.02 Å when spin−orbit coupling is included.[52] The structures of the SOC ground states of uranocene and plutonocene (sections 3.3 and 3.4) suggest that a small SOF basis would be suitable for capturing the majority of the spin−orbit coupling contribution to the total energy, thereby allowing us to address the equilibrium ring-metal separations at this level. For uranocene, we coupled the ^3A_g, $^3B_{1g}$, $^3B_{2g}$, and $^3B_{3g}$ SOF states (in the full calculations, these states make up 95.1% of the SOC ground state at the SOF equilibrium geometry). For plutonocene, we coupled the ^5A_g, $^5B_{2g}$, and $^5B_{3g}$ SOF states (which give 88.8% of the SOC ground state at the SOF equilibrium geometry). Figure 10 shows the potential energy curves for the metal-ring centroid distance for both the SOF and SOC states for these two systems. The effects of spin−orbit coupling on the calculated geometries are minimal; for uranocene, the equilibrium ring-metal separation increases slightly from 1.944 to 1.945 Å, while for plutonocene the separation remains unchanged to within 0.001 Å at 1.898 Å. These small variations (in line with those found in ref 49 at the same level of theory) show that, while spin−orbit coupling has a large effect on the energies and electronic structures of these systems, the geometrical structures are largely unaffected, and so our choice of using spin−orbit coupling free geometries for the majority of the calculations presented here is justified.

4. Summary and Discussion

In this contribution we have presented SOF- and SOC-CASPT2 calculations on thorocene, uranocene, plutonocene, and curocene, with the principal aim of establishing if the ground-state electronic structures of the later examples can be characterized in the same manner as the lanthanocenes, and in particular cerocene. The method used here is particularly well suited to this task; spin−orbit coupling effects are weak among the lanthanides and indeed are almost nonexistent for the cerocene ground state. By contrast, spin−orbit coupling is strong among the open-shell actinides, and so our expression of the SOC ground state in terms of an SOF basis allows for a clear comparison to be made. Our good agreement with previous work on thorocene and uranocene indicates that the SOC-CASPT2 method is an appropriate method for such studies.

In our previous calculations on thorocene and cerocene,[22] we concluded that the main difference between the ground-state electronic structures of the two is the significantly noninteger occupation of the a_u/b_{1u} (e_{2u}) levels in cerocene. This in turn leads to a large value of the f density (n_f) for this system. In the present calculations we find a systematic increase in the fractional occupancies of these levels in the SOF ground states

as the actinide series is crossed. By the time plutonium is reached, the fractional occupations are very close to those found in cerocene and increase again in curocene.

Although spin−orbit coupling makes little difference to the equilibrium geometry of uranocene and plutonocene, it has a significant effect on the energy spectrum of all the systems considered here other than thorocene. However, the SOF ground states make the dominant contribution to their SOC counterparts. We therefore conclude that the electronic structures of the later actinocenes can indeed be interpreted in the same manner as cerocene.

The SOF ground states also give us a clear understanding of how the 5f levels are filled in these systems. Thorocene has an empty f shell (and excited states favor a $6d_\sigma^1$ occpuation), while the uranocene ground state favors a triplet $f_\pi^1 f_\phi^1$ configuration. Plutonocene follows this trend, favoring a quintet $f_\pi^2 f_\phi^2$ occupation. For the two latter systems we find low-lying excited states, as would be expected when the large density of states associated with f^2 and f^4 metal configurations is considered. The situation is markedly different in curocene, which is forced to occupy a high-lying f_δ level even when in a tetravalent oxidation state. An f^6 metal configuration in this system precludes any low-lying excited SOF states, and this is indeed what is found.

Finally, we draw attention to our SOC plutonocene ground state. Plutonocene has been the center of a great deal of theoretical attention, due in large part to its magnetic behavior; originally characterized as diamagnetic,[4] it was later shown[12] to exhibit TIP. The TIP dictates that the ground state must have $|M_J| = 0$ and therefore be nondegenerate, as has been shown to be likely from crystal-field studies,[4,42,43] and indeed has been found at the SOCI level.[36] We are therefore pleased to be able to confirm these previous findings using the present, more sophisticated approach.

Acknowledgment. We are grateful to the EPSRC for supporting this work via grants EP/C533054 and GR/S06233 and for the use of its National Service for Computational Chemistry Software (http://www.nsccs.ac.uk). We also thank UCL for computing resources via the Research Computing "Legion" cluster and associated services.

Supporting Information Available: Tables showing percentage contribution from $ThCOT_2$, $UCOT_2$, $PuCOT_2$, and $CmCOT_2$ SOF states to the low-lying SOC states. This material is available free of charge via the Internet at http://pubs.acs.org.

References and Notes

(1) Streitwieser, A.; Kinsley, S. A.; Rigsbee, J. T.; Fragala, I. L.; Ciliberto, E.; Rosch, N. *J. Am. Chem. Soc.* **1985**, *107*, 7786.
(2) Avdeef, A.; Zalkin, A.; Raymond, K. N.; Hodgson, K. O. *Inorg. Chem.* **1972**, *11*, 1083.
(3) Streitwieser, A. J.; Müller-Westerhof, U. *J. Am. Chem. Soc.* **1968**, *90*, 7364.
(4) Karraker, D. G.; Stone, J. A.; Jones, E. R.; Edelstein, N. M. *J. Am. Chem. Soc.* **1970**, *92*, 4841.
(5) Solar, J. P.; Burghard, H. P. G.; Banks, R. H.; Streitwieser, A. J.; Brown, D. *Inorg. Chem.* **1980**, *19*, 2186.
(6) Dallinger, R. F.; Stein, P.; Spiro, T. G. *J. Am. Chem. Soc.* **1978**, *100*, 7865.
(7) Zalkin, A.; Raymond, K. N. *J. Am. Chem. Soc.* **1969**, *91*, 5667.
(8) Streitwieser, A.; Müller-Westerhoff, U.; Sonnischen, U. G.; Mares, D. G.; Hodgson, K. O.; Harmon, C. A. *J. Am. Chem. Soc.* **1973**, *95*, 8644.
(9) Karraker, D. G. *Inorg. Chem.* **1973**, *12*, 1105.
(10) Clark, J. P.; Green, J. C. *J. Chem. Soc., Dalton Trans.* **1977**, 505.
(11) Brennan, J. B.; Green, J. C.; Redfern, C. M. *J. Am. Chem. Soc.* **1989**, *111*, 2373.
(12) Eisenberg, D. C.; Streitwieser, A.; Kot, W. K. *Inorg. Chem.* **1990**, *29*, 10.
(13) Edelstein, N. M.; Allen, P. G.; Bucher, J. J.; Shuh, D. K.; Sofield, C. D.; Kaltsoyannis, N.; Maunder, G. H.; Russo, M. R.; Sella, A. *J. Am. Chem. Soc.* **1996**, *118*, 13115.
(14) Booth, C. H.; Walter, M. D.; Daniel, M.; Lukens, W. W.; Andersen, R. A. *Phys. Rev. Lett.* **2005**, 95.
(15) Riseborough, P. S. *Adv. Phys.* **2000**, *49*, 257.
(16) Kotani, A.; Mizuta, H.; Jo, T.; Parlebas, J. C. *Solid State Commun.* **1985**, *53*, 805.
(17) Gilbert, A.; Vidhyadhiraja, N. S.; Logan, D. E. *J. Phys.: Condens. Matter* **2007**, 19.
(18) Streitwieser, A.; Kinsley, S. A.; Jenson, C. H.; Rigsbee, J. T. *Organometallics* **2004**, *23*, 5169.
(19) Dolg, M.; Fulde, P.; Stoll, H.; Preuss, H.; Chang, A.; Pitzer, R. M. *Chem. Phys.* **1995**, *195*, 71.
(20) Amberger, H. D.; Reddmann, H.; Edelmann, F. T. *J. Organomet. Chem.* **2005**, *690*, 2238.
(21) Walter, M. D.; Booth, C. H.; Lukens, W. W.; Andersen, R. A. *Organometallics* **2009**, *28*, 698.
(22) Kerridge, A.; Coates, R.; Kaltsoyannis, N. *J. Phys. Chem.* **2009**, *113*, 2896.
(23) Kaltsoyannis, N.; Scott, P. *The f elements*; Oxford University Press: Oxford, 1999.
(24) Dolg, M.; Fulde, P. *Chem.−Eur. J.* **1998**, *4*, 200.
(25) Karlstrom, G.; Lindh, R.; Malmqvist, P. A.; Roos, B. O.; Ryde, U.; Veryazov, V.; Widmark, P. O.; Cossi, M.; Schimmelpfennig, B.; Neogrady, P.; Seijo, L. *Comput. Mater. Sci.* **2003**, *28*, 222.
(26) Douglas, M.; Kroll, N. M. *Ann. Phys.* **1974**, *82*, 89.
(27) Roos, B. O. Unpublished results.
(28) Hunt, W. J.; Goddard, W. A. *Chem. Phys. Lett.* **1969**, *3*, 414.
(29) Dolg, M.; Fulde, P.; Kuechle, W.; Neumann, C. S.; Stoll, H. *J. Chem. Phys.* **1991**, *94*, 3011.
(30) Frisch, M. J.; Trucks, G. W.; Schlegel, H. B.; Scuseria, G. E.; Robb, M. A.; Cheeseman, J. R.; Montgomery, J. A., Jr.; Vreven, T.; Kudin, K. N.; Burant, J. C.; Millam, J. M.; Iyengar, S. S.; Tomasi, J.; Barone, V.; Mennucci, B.; Cossi, M.; Scalmani, G.; Rega, N.; Petersson, G. A.; Nakatsuji, H.; Hada, M.; Ehara, M.; Toyota, K.; Fukuda, R.; Hasegawa, J.; Ishida, M.; Nakajima, T.; Honda, Y.; Kitao, O.; Nakai, H.; Klene, M.; Li, X.; Knox, J. E.; Hratchian, H. P.; Cross, J. B.; Bakken, V.; Adamo, C.; Jaramillo, J.; Gomperts, R.; Stratmann, R. E.; Yazyev, O.; Austin, A. J.; Cammi, R.; Pomelli, C.; Ochterski, J. W.; Ayala, P. Y.; Morokuma, K.; Voth, G. A.; Salvador, P.; Dannenberg, J. J.; Zakrzewski, V. G.; Dapprich, S.; Daniels, A. D.; Strain, M. C.; Farkas, O.; Malick, D. K.; Rabuck, A. D.; Raghavachari, K.; Foresman, J. B.; Ortiz, J. V.; Cui, Q.; Baboul, A. G.; Clifford, S.; Cioslowski, J.; Stefanov, B. B.; Liu, G.; Liashenko, A.; Piskorz, P.; Komaromi, I.; Martin, R. L.; Fox, D. J.; Keith, T.; Al-Laham, M. A.; Peng, C. Y.; Nanayakkara, A.; Challacombe, M.; Gill, P. M. W.; Johnson, B.; Chen, W.; Wong, M. W.; Gonzalez, C.; Pople, J. A. *Gaussian 03*, revision C.02; Gaussian, Inc.: Wallingford, CT, 2004.
(31) MOLCAS Version 6.4 User's Manual Lund University, 2006, 129.
(32) Lowdin, P. O. *Phys. Rev.* **1955**, *97*, 1474.
(33) Malmqvist, P. A.; Roos, B. O.; Schimmelpfennig, B. *Chem. Phys. Lett.* **2002**, *357*, 230.
(34) Liu, W. J.; Dolg, M.; Fulde, P. *J. Chem. Phys.* **1997**, *107*, 3584.
(35) Chang, A. H. H.; Pitzer, R. M. *J. Am. Chem. Soc.* **1989**, *111*, 2500.
(36) Chang, A. H. H.; Zhao, K.; Ermler, W. C.; Pitzer, R. M. *J. Alloys Compd.* **1994**, *213/214*, 191.
(37) Kot, W. K.; Shalimoff, G. V.; Edelstein, N. M.; Edelman, M. A.; Lappert, M. F. *J. Am. Chem. Soc.* **1988**, *110*, 986.
(38) Kaltsoyannis, N.; Bursten, B. E. *J. Organomet. Chem.* **1997**, *528*, 19.
(39) Schmidt, M. W.; Gordon, M. S. *Annu. Rev. Phys. Chem.* **1998**, *49*, 233.
(40) Levanda, C.; Streitwieser, A. *Inorg. Chem.* **1981**, *20*, 656.
(41) Shannon, R. D. *Acta Crystallogr., Sect. A* **1976**, *32*, 751.
(42) Hayes, R. G.; Edelstein, N. M. *J. Am. Chem. Soc.* **1972**, *94*, 8688.
(43) Warren, K. D. *Inorg. Chem.* **1975**, *14*, 3095.
(44) *The Chemistry of the Actinide and Transactinide Elements*, 3rd ed.; Morss, L. R., Edelstein, N. M., Fuger, J., Eds.; Springer: Dordrecht, 2006.
(45) Asprey, L. B.; Ellinger, F. H.; Fried, S.; Zachariasen, W. H. *J. Am. Chem. Soc.* **1955**, *77*, 1707.
(46) Peterson, J. R.; Fuger, J. *J. Inorg. Nucl. Chem.* **1971**, *33*, 4111.
(47) Prodan, I. D.; Scuseria, G. E.; Martin, R. L. *Phys. Rev. B* **2007**, 76.
(48) Menconi, G.; Kaltsoyannis, N. *Chem. Phys. Lett.* **2005**, *415*, 64.
(49) Clavaguera-Sarrio, C.; Vallet, V.; Maynau, D.; Marsden, C. J. *J. Chem. Phys.* **2004**, *121*, 5312.
(50) La Macchia, G.; Infante, I.; Raab, J.; Gibson, J. K.; Gagliardi, L. *Phys. Chem. Chem. Phys.* **2008**, *10*, 7278.
(51) Groen, C. P.; Varga, Z.; Kolonits, M.; Peterson, K. A.; Hargittai, M. *Inorg. Chem.* **2009**, *48*, 4143.
(52) Vetere, V.; Maldivi, P.; Adamo, C. *J. Comput. Chem.* **2003**, *24*, 850.

JP903912Q